SHAKE TABLE TEST OF A 2-STOREY STEEL BUILDING SEISMICALLY RETROFITTED USING GRAVITY-CONTROLLED ROCKING BRACED FRAME SYSTEM

Paul Mottier[1], Robert Tremblay[2], and Colin Rogers[3]

[1]Graduate Researcher, [2]Professor, Department of Civil, Geological and Mining Engineering, Polytechnique Montreal, Montreal, Canada
[3]Professor, Department of Civil Engineering and Applied Mechanics, McGill University, Montreal, Canada
Contact: paul.mottier@gadz.org

This article describes a shake-table test program that was conducted to investigate the seismic behaviour of a half-scale two-storey gravity-controlled rocking braced steel frame building. In this system, braced frame columns are designed to uplift from the foundation under severe earthquakes to reduce the seismic force demands on the frame members. Self-centering capacity is solely provided by the gravity loads carried by the rocking frame. Energy dissipative devices are added at the base of the braced frame columns to control drifts. The system can be used for new structures as well as the retrofit of seismically deficient structures. In the test program, the specimen represented a gravity-controlled rocking frame that had been proposed for seismic retrofit in a previous study. The test structure was subjected to ground motions expected for two site classes in two seismically active regions in Canada. Three different energy dissipative devices located at the rocking interface were studied: friction, friction spring dampers, and steel bars yielding in tension and elastically buckling in compression. The focus of the tests was on peak axial loads in the columns and additional moments and shears in the beams resulting from column impact upon rocking. Axial loads in the braces and columns from higher mode response were also examined. The tests revealed significant increases in beam forces due to column impacts. Large axial forces due to the second vibration mode response were measured in the second storey braces. A numerical model is proposed to accurately predict the measured force demands.

KEYWORDS

Shake table testing; Braced steel frame; Rocking; Retrofit; Column impact

INTRODUCTION

The use of controlled rocking braced steel frames to enhance the seismic performance of building structures has been studied since the 1960s (Housner 1963; Huckelbridge 1977; Kelly and Tsztoo 1977, Priestley 1978, Tran et al. 2004, Midorikawa et al. 2006, Tremblay et al. 2008, Pollino and Bruneau 2008, 2010, Deierlein et al 2010, Sause et al. 2010, Deierlein et al 2011, Wiebe et al. 2013, Eatherton and Hajjar 2014, Eatherton et al. 2014, Dyanati et al. 2015, Hogg 2015, Jahnel and Cole 2017, Steele and Wiebe 2017, Mottier et al. 2017, Binder and Christopoulos 2018). In such structures, the columns of the braced frame can uplift from their foundations during a severe earthquake to reduce seismic induced forces in the structures. Self-centering response is achieved by means of the gravity loads supported by the frame, vertical post-tensioning, yielding base plates, ring springs, or a combination of these elements. Energy dissipation (ED) mechanisms are typically introduced in the system to control lateral drifts. These ED mechanisms can be placed between the uplifting columns and adjacent gravity columns or at the base of the rocking frame columns. Past numerical and experimental studies have shown that rocking systems can significantly reduce seismic induced member forces, while exhibiting uniform and limited displacements over the building height. More importantly, rocking frames can withstand severe earthquakes with no or minimal structural damage. To date, rocking braced frame systems have been implemented in bridge and building structures (Dowdell and Hamersley 2000, Tipping-Mar 2012, Latham et al. 2013) and have exhibited satisfactory performance during significant earthquakes (Hogg 2015).

In previous studies, rocking braced frames were generally implemented independently from the gravity load resisting system to avoid imposing vertical displacements to the adjacent building structure. In such uncoupled rocking braced frames, the rocking frame only carries its own weight, and self-centering capacity of the system must be provided by vertical post-tensioned tendons anchored to the foundations. For low-rise building applications, post-tensioned tendons may not permit the required elastic elongation capacity because of their shorter lengths (Mar 2010). To overcome this difficulty, it has been proposed to construct the rocking frame with the gravity framing system, and as such to make use of the gravity loads supported by the frame to develop a self-centering capacity. Past shake table and numerical studies have indicated that the restoring capacity provided solely from gravity loads could be sufficient to achieve adequate seismic performance, even in regions of high seismicity (Huckelbridge 1977; Kelly and Tsztoo 1977, Tran et al. 2004, Midorikawa et al. 2006, Tremblay et al. 2008, Pollino and Bruneau 2010, Mottier et al. 2017). This gravity-controlled rocking frame (GCRBF) system is the focus of the study presented in this paper.

Mottier et al. (2017) numerically investigated the feasibility of using GCRBFs for the seismic retrofit of 2- and 3-storey seismically deficient steel chevron braced frame structures. Figure 1a shows the two-storey building structure located on a class E site (soft soil) in Vancouver, British Columbia, that was examined in that study. The retrofit scheme consisted of allowing column uplift while maintaining base shear resistance by removing the anchor rods, adding horizontal restraints (blockers) against the outer edges of the base plates, and introducing vertical ED devices between the columns and the foundation. A horizontal strut was also introduced between the two columns near their bases. Three ED systems were considered in the study: friction, ring springs, and steel bars yielding in tension and elastically buckling in compression (Figure 2).

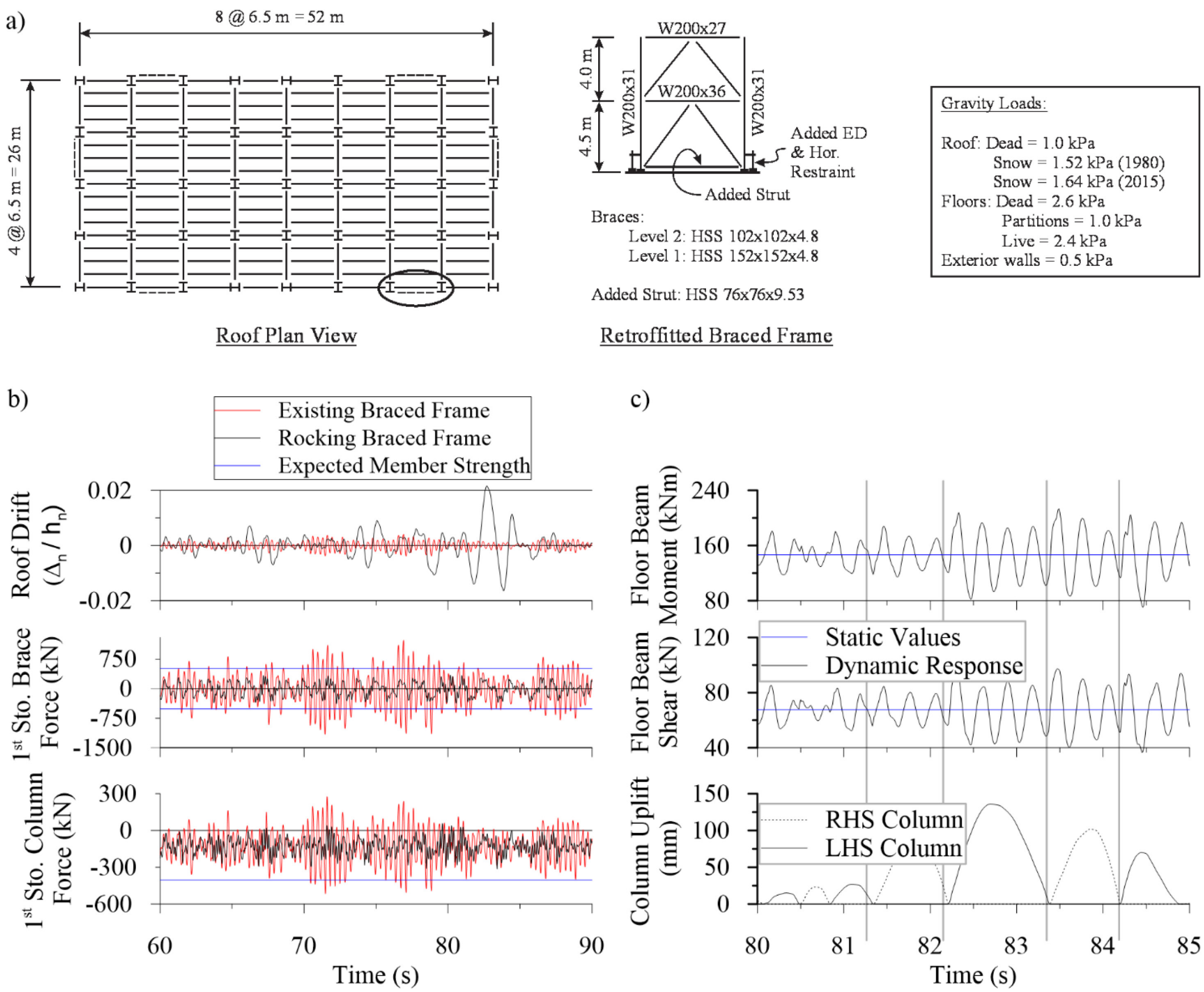

Figure 1 Prototype two-storey building studied by Mottier et al.: a) Structure with retrofitted rocking braced frames; b) Histories of the brace and column axial loads and the roof drift for the existing and rocking braced frames (GCRBF with friction ED); c) Histories of the bending moments and shears in the first-storey beam and of the column uplift for the GCRBF with friction ED elements.

In Figure 1b, the benefits of allowing braced frame rocking on axial load demands on braces and columns can be clearly observed for one of the ground motions considered. In the figure, the roof displacements for the rocking braced frame remained within 1% of the building height, and the study showed that this retrofit scheme could substantially improve the building seismic performance based on the ASCE 41-13 criteria (ASCE, 2014). As shown in Figure 1c, however, the numerical simulations revealed that column impacts upon rocking could induce significant additional flexural and shear demands on the floor beams framing into the uplifting columns. This phenomenon was observed in past shake table tests by Huckelbridge (1977) and Pollino and Bruneau (2010). These tests revealed vertical accelerations reaching up to 4*g* (*g* is the acceleration due to gravity) shortly after column impacts. More recently, Mottier et al. (2019) performed lift and release tests on an individual column supporting beams with masses. The tests confirmed high acceleration demand (up to 8*g*) as well as significant increases in beam shears and bending moments, as those shown in Figure 1c. These additional forces need to be assessed, to better understand the behaviour of GCRBFs structures.

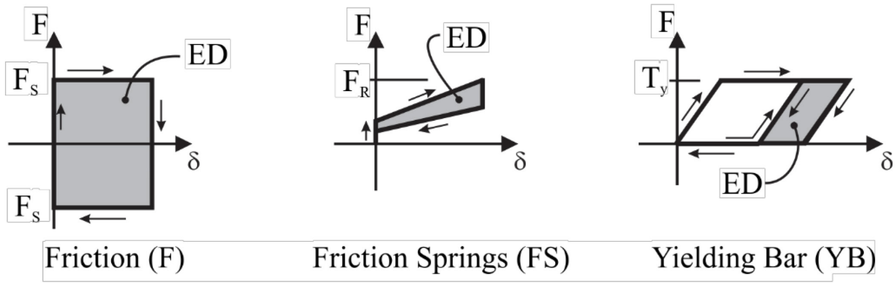

Figure 2 Theoretical responses of the studied energy dissipation devices.

This article presents a shake table test program that was conducted to confirm the numerical findings obtained by Mottier et al. (2017). The main objective of the investigation was to evaluate the force demands in frame members from vertical accelerations and inertia forces induced by impacts between the rocking frame columns and the foundations, in order to confirm that numerical models can predict the additional force demands properly and the overall behaviour of the system. The experimental program was conducted on the unidirectional earthquake simulator of the Structural Engineering Laboratory at Polytechnique Montréal. The tests were performed on half-scale models developed from the two-storey buildings studied by Mottier et al. The specimens were subjected to ground motions expected for soft rock (class C) site in Montreal, Quebec, as well as soft rock and soft soil (classes C and E) sites in Vancouver, British Columbia. These two locations are representative of the seismic regions in eastern and western Canada, respectively. Energy dissipation from friction, ring springs, and steel bars yielding in tension were also examined in the tests.

The test program is first described, including a presentation of the test specimens and applied ground motions. The results from preliminary testing conducted to obtain the dynamic properties of the test frames are presented. The frame response to an individual earthquake ground motion is detailed and discussed. The relative efficiency of the three ED mechanisms for displacement control are compared. This is followed by a presentation of the effects of column impacts expressed as a function of column uplift amplitudes for all tests performed for both locations studied. Finally, a numerical model of the experiment is described and comparisons between experimental and numerical results are presented and discussed.

EXPERIMENTAL PROGRAM

Test specimens

The unidirectional earthquake simulator at Polytechnique Montréal has 3.4 m x 3.4 m plan dimensions and 10 m clear test height. It is driven by a 500 kN high performance hydraulic actuator. The tests were performed on a half-scale model of prototype frames adapted from the 6.5 m wide two-storey frames studied by Mottier et al. (2017). The test frame shown in Figure 3 was used for the prototypes located in both Montreal and Vancouver. Only the seismic weight was varied to reflect the seismic loads applicable to each location, as explained later. In the prototype structures, the braced frames were located along the exterior walls. For the model in the laboratory, gravity framing was placed on both sides of the specimen to avoid in-plane torsional response (Figure 4). Stacks of 19.1- and 25.4-mm thick steel plates were placed on this framing to apply gravity loads on the rocking braced frame. The plates within each stack were welded together along their sides to behave as a single unit. They were also firmly tightened to the floor and roof beams to act compositely with the framing members. Angles were also used to prevent any slippage during the tests.

As shown in Figure 4b, the width of the gravity framing extended beyond the shake table. As such, the test specimen had to be mounted on two 5 m long transverse supporting HSS 203x203x13 beams secured to the earthquake simulator using 25 mm pre-tensioned high-strength bolts. The vertical displacement of the supporting beams was not measured. The test specimens were laterally braced in the out-of-plane direction by a pair of horizontal HSS members placed on either side of the rocking braced frame at mid-height of the second level. Frictionless PTFE shims were used between these HSS members and the rocking frame columns to minimize frictional resistance. Additional out-of-plane bracing, as shown on the top of Figure 4a, was used to avoid any torsional effects during the test.

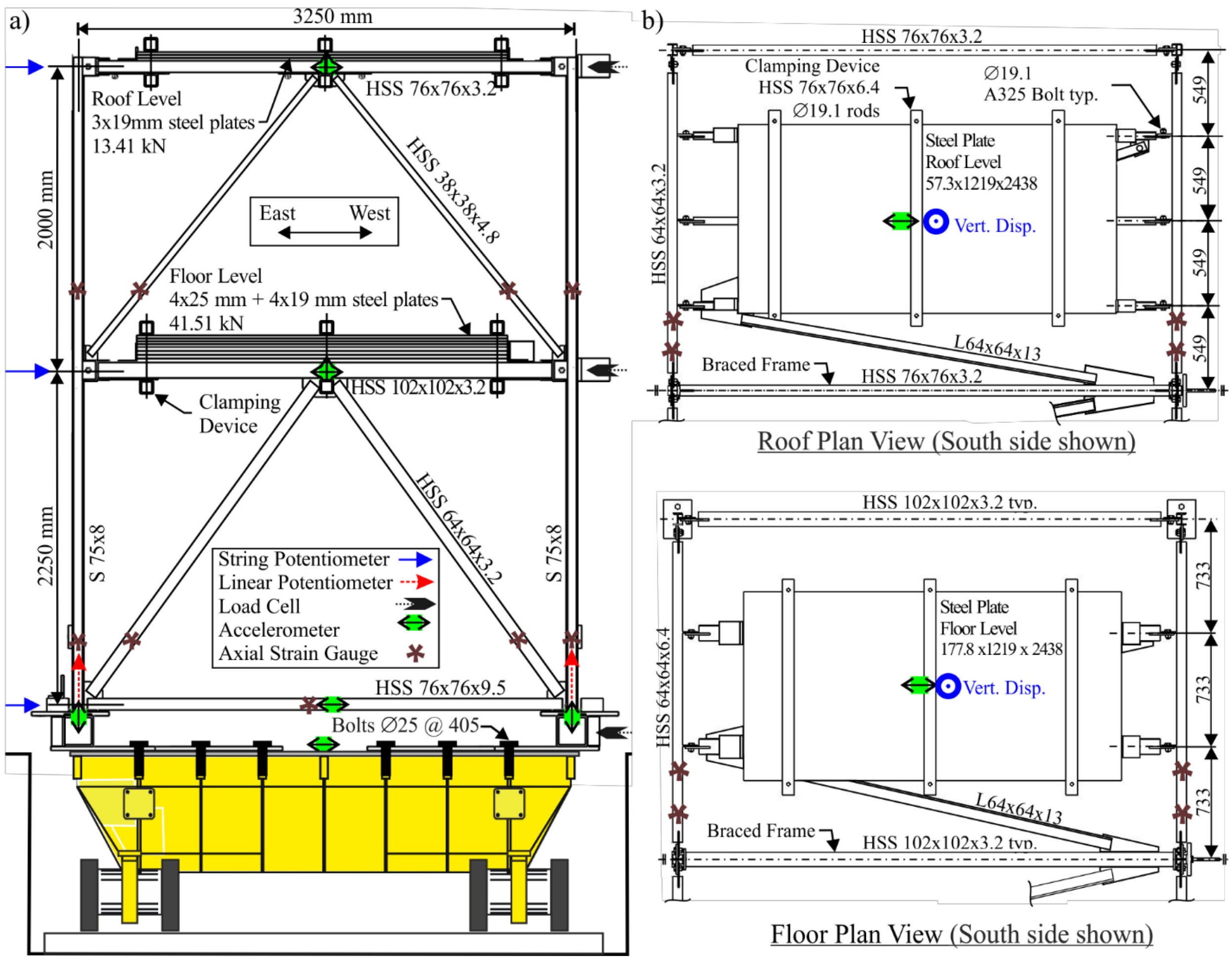

Figure 3 Rocking brace frame specimen with construction and instrumentation details: a) Rocking frame elevation (from North); b) Half plan views of the floor and roof structures.

The test specimen was built from structural steel, which was designed to satisfy the applicable similitude laws, as was done in previous studies (Tremblay et al., 2008; Wiebe et al, 2013). The scaling factors used are detailed in Table 1, in which subscript $_m$ refers to the model, and subscript $_p$ refers to the prototype.

Table 1 Scaling factors used in the design of the test specimen

Scaling Factors	Length	Stress	Time	Force	Horizontal Accelerations	Seismic Weight
	$\alpha = L_m/L_p$	$\beta = \sigma_m/\sigma_p$	$\gamma = t_m/t_p$	$S_F = \alpha^2\beta$	$S_{HA} = \alpha/\gamma^2$	$S_{SW} = \alpha\beta\gamma^2$
	0.5	1.0	0.3	0.25	5.56	0.045

Time was reduced by a factor $\gamma = t_m/t_p = 0.3$ to decrease the required seismic weight, which allowed for the use of the existing shake table test facility. Acceleration due to gravity could not be modified and the number and sizes of the steel plates replicating floor and roof gravity loads were determined to impose on the rocking frame the gravity loads required from the application of the similitude laws. For the tests performed for the Vancouver location, these gravity loads also approximately reproduced the horizontal seismic weights required with the S_{HA} scale factor. For the tests representing the Montreal conditions, the same gravity loads were kept but the seismic weight had to be increased to satisfy similitude requirements. This was achieved by using a seismic weight system located next to the earthquake simulator (Figure 4b). This system consisted of a steel frame supporting steel plates that were connected to the test specimen at every level. Columns in the seismic weight system had carefully machined rocker connections at their top and bottom ends such that the frame offered no lateral resistance in the direction of testing. The seismic weight system was placed on a horizontal frame which was mounted on rollers and secured to the shake table so that the system experienced the same ground motion as the test specimen. Load cells were used in the horizontal struts connecting the steel plates of the seismic weight system to the test specimen so that inertia loads could be directly monitored during the tests.

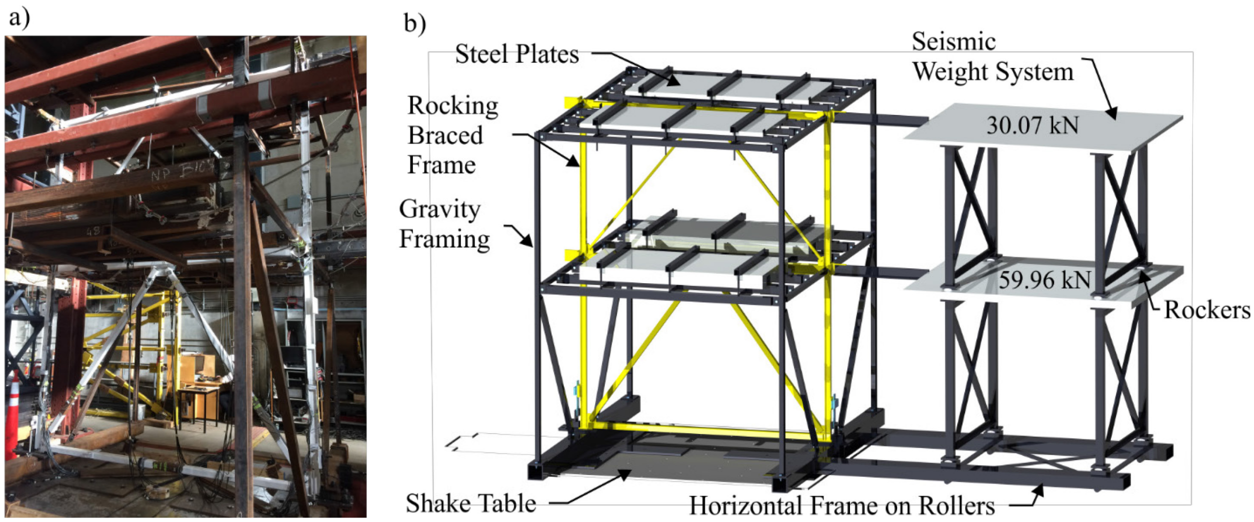

Figure 4 Test Setup: a) Test specimen with gravity frame on the shake table; b) 3D view of the test specimen and the seismic weight system for the Montreal location.

As designed, the total vertical load resisted by each column of the test rocking brace frame was equal to 28 kN. Assuming the vertical distribution of the seismic loads specified in the equivalent static force procedure of the 2015 National Building Code of Canada (NBCC) (NRCC 2015), column uplift of the rocking braced frame including the resistance from gravity loads would initiate under a total earthquake load (base shear) of 44 kN. The sections of the beams supporting the gravity loads were sized to obtain the vertical frequencies of the roof and floor systems of the prototype structures after applying the time scale factor. The beams were connected to the columns through one-bolt shear-tab connections, as illustrated in Figure 5b. For clarity, only one floor beam connection detail is shown in the figure. The bolt in each connection was manually torqued at the beginning of each test to achieve a pinned condition at the beam ends. Details of the rocking braced frame column base are illustrated in Figure 5a. The columns had welded rectangular base plates, as is commonly done in practice. The base plates were seated on a 25 mm thick foundation plate welded to the HSS 203x203x13 beams supporting the test specimen. No anchor rods were used to simulate the prototype structures in the retrofitted condition. Horizontal reaction blocks made with HSS 89x89x13 were placed on the exterior side of each column to resist base shear. These HSS blocks were designed with a 10 mm thick vertical plate bearing against the edge of the column base plate, a detail that was successfully tested in previous experimental studies (Wiebe et al. 2013; Eatherton and Hajar 2014). The blocker was held in place by the 35 mm threaded rod connecting the ED devices with a safety edge plate placed behind it to prevent slippage during the tests. The contact surfaces between the column base plate and the blocker were greased to reduce friction during column uplift. As required in the retrofit scheme of Figure 1a, a horizontal strut was also placed between the two columns to maintain column spacing and transfer horizontal components of the brace forces upon rocking.

The base supporting the rocking columns was also detailed to allow the placement of the three ED mechanisms of Figure 2. Figure 6 shows photographs and schematic drawings of the base rocking joints in the three configurations. As depicted in the figures, the ED mechanisms are referred to as F for the friction device, FS for the friction springs and YB for the yielding bar. All three EDs were sized to develop a 12.5 kN activation force, i.e. 45% of the column gravity load. The F mechanism consisted of steel plates connected with a single-shear bolted lap splice including 6.35

mm thick abrasion resistant SSAB Hardox 500 steel shim plates with a nominal hardness of 500 HBW and connected with one 16 mm diameter A325 bolt. The bolt was torque-control tightened to achieve a slip resistance of 12.5 kN. The FS device was fabricated using a series of 76 springs no. 05500 by RINGFEDER® to obtain a stiffness of 0.4 kN/mm. The springs were pre-compressed under a force of 4.0 kN, which left 54.3 mm deformation capacity after activation. The YB system consisted of a 2.65 mm x 38 mm x 1500 mm long ASTM A1011 steel plate (F_y of 325 MPa), which was bolted at both ends. All three devices were connected to the HSS blocker and the 25 mm foundation plate by means of one 35 mm diameter threaded bar. This connection was stiffened by means of two 13 mm x 76 mm vertical plates welded to the side of the HSS 203x203x13 beam and the underside of the 25 mm foundation plate.

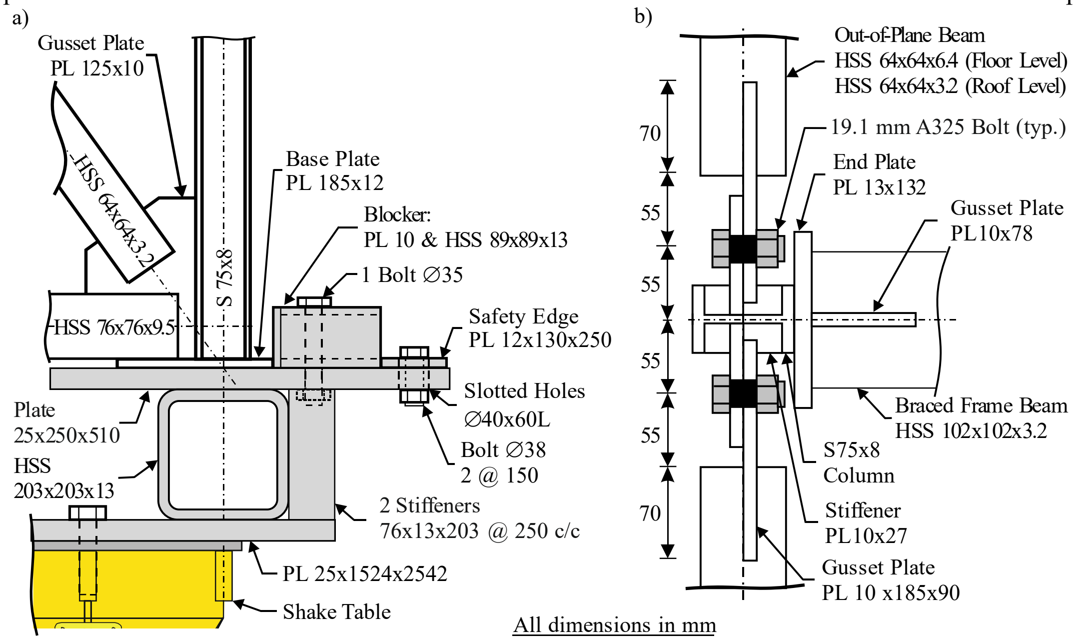

Figure 5 Construction details: a) Beam-to-column shear tab connections at the floor level (view from top); b) Elevation of the rocking column base (ED not shown – see Fig. 6).

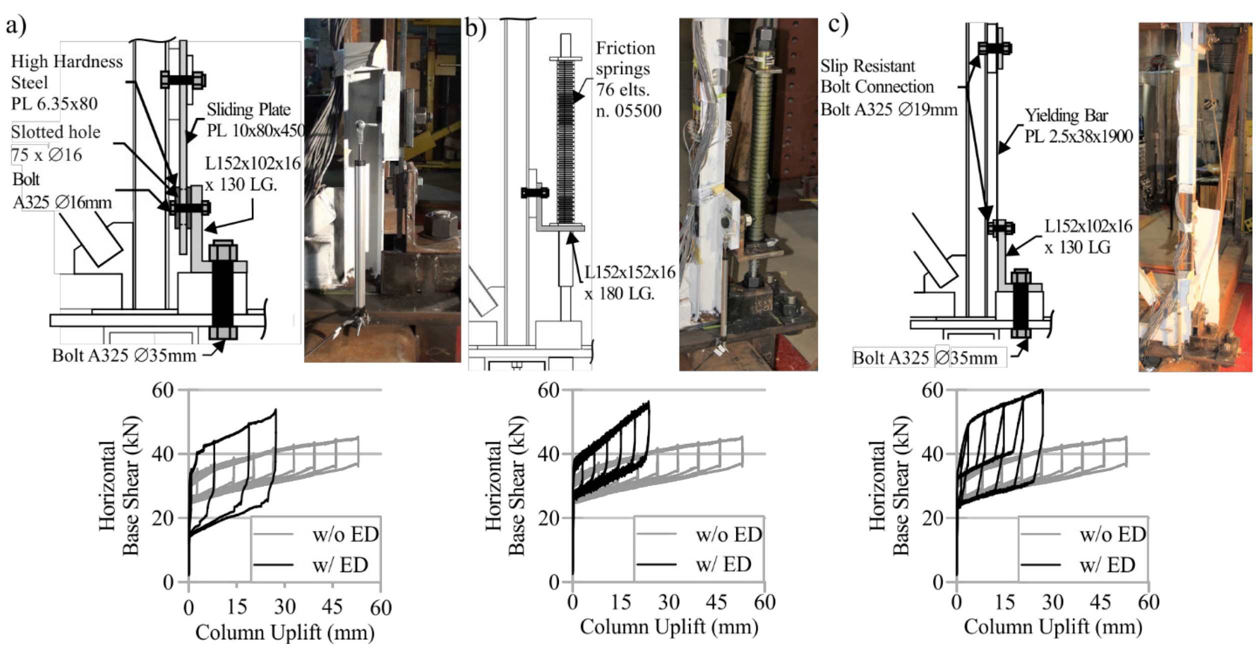

Figure 6 Details of the ED devices and measured rocking frame hysteretic responses: a) Friction (F); b) Friction Springs (FS); and c) Yielding Bar (YB).

Figure 6 also shows the base shear *vs* column uplift responses of the rocking frames with the three ED devices as measured during the quasi-static cyclic tests performed on the rocking braced frame prior to the seismic shake table tests. The results of said tests are discussed later.

Instrumentation

Figure 3 shows details and locations of the sensors that were used in the test program. Two 50g-accelerometers were placed on the base plates of the rocking columns to measure the vertical accelerations induced during the impacts. Six 10g-accelerometers were used to measure vertical and horizontal accelerations at different locations : one horizontal accelerometer at the strut mid-length at the base of the frame, pairs of vertical and horizontal accelerometers at mid-span of the rocking frame beams at floor and roof levels, and a horizontal accelerometer installed on the shake table to monitor the acceleration applied to the specimen. Two horizontal 5g-accelerometers were also installed on top of the steel plate assemblies supported by the gravity framing at the floor and roof levels. Two linear potentiometers were installed at the base of each rocking column, one for measuring possible out-of-plane lateral displacements of the frame and one for measuring uplift of the columns upon rocking. String potentiometers were mounted at each level of the frame to capture the longitudinal horizontal displacements of the frame. Four pairs of string-potentiometers were also positioned to obtain the vertical displacements of the centre of each steel plate assembly from in-plane triangulation, at each level and on both sides of the rocking frame, as indicated by the blue circles in Figure3 b. Strain gauges were placed on the columns and braces to measure axial loads in these members at both levels. Strain gauges were also placed on gravity load supporting beams framing into the RBF columns to measure the bending moments and shears in these primary members. Bending moments in these beams were measured at two positions along the beam length, as shown in Figure 3 b, and shears near the beam ends could be obtained from the moment gradients between these two positions. All data was recorded using an HBM synchronized data acquisition system and processed with Catman DAQ software (HBM, 2000). An acquisition rate of 600 Hz was used during the seismic tests.

Test Program

The experimental program included two phases. The first phase included preliminary white noise base excitation, pull-release tests and quasi-static cyclic tests performed to characterize the static and dynamic properties of the test specimen. The second phase included the seismic tests. The ground motion records used in the prototype buildings studied in (Mottier et al., 2017) for each location and site conditions for the second phase of tests are given in Table 2. Their 5% damped acceleration response spectra are shown in Figure 7, in which the grey area represent the period ranges used for scaling.

Table 2 Details of the ground motions signals used in the seismic tests

GM ID	Type	Earthquake	Mw	Record	R (km)	Site Class	Comp(°).	SF1	SF2	% Applied	ED Device
MC1	Crustal	Simulated	6.0	Trial 1	12.8	C	239.3	0.55	1.03	60	F; FS
MC2	Crustal	Simulated	6.0	Trial 2	16.9	C	41.0	0.90	1.03	70	F; FS
MC5	Crustal	Simulated	6.0	Trial 2	24.4	C	78.7	1.60	1.03	70	F; FS
MC7	Crustal	Simulated	7.0	Trial 1	20.1	C	126.4	0.59	1.03	40	F; FS
MC8	Crustal	Simulated	7.0	Trial 3	25.6	C	276.5	0.69	1.03	60	F; FS; YB
MC9	Crustal	Simulated	7.0	Trial 1	41.6	C	304.4	1.31	1.03	50	F; FS
MC10	Crustal	Simulated	7.0	Trial 2	45.2	C	85.6	1.61	1.03	50	F; FS
MC11	Crustal	Simulated	7.0	Trial 2	98.6	C	157.7	1.98	1.03	50	F; FS; YB
VC01	Crustal	1971 San Fernando	6.61	Castaic - Old Ridge Route	23	C	291	1.39	1.2	30	F; FS
VC06	Crustal	1994 Northridge	6.69	Castaic - Old Ridge Route	21	C	90	0.66	1.2	40	F; FS
VC19	In-Slab	13/01/2001 El Salvador	7.6	6987c	70	C	360	2.01	1.2	40	F; FS
VC21	In-Slab	13/01/2001 El Salvador	7.6	7147c	93	C	180	4.81	1.2	40	F; FS
VC30	Interface	11/03/2011 Tohoku, Japan	9	IBR008	161	C	NS	2.32	1.2	40	F; FS; YB
VC32	Interface	11/03/2011 Tohoku, Japan	9	YMT009	156	C	EW	2.77	1.2	40	F; FS; YB
VE01	Crustal	1979 Imperial Valley-06	6.53	El Centro Array #12	18	E	140	3.44	1.125	30	F; FS; YB
VE29	Crustal	2010 El Mayor-Cucapah_ Mexico	7.20	El Centro Array #12	11	E	90	1.15	1.125	30	F; FS
VE31	In-Slab	28/02/2001 Nisqually	6.80	0730a	45	E	180	2.19	1.125	25	F; FS
VE34	In-Slab	24/03/2001 Japan	6.80	EHM003	50	E	NS	2.05	1.125	40	F; FS
VE43	Interface	11/03/2011 Tohoku, Japan	9.00	AKT006	159	E	NS	7.22	1.125	35	F; FS; YB
VE48	Interface	11/03/2011 Tohoku, Japan	9.00	FKS020	155	E	NS	1.34	1.125	25	F; FS
VE52	Interface	26/09/2003 Tokachi-Oki, Japan	8.00	YMTH02	155	E	NS	3.35	1.125	35	F; FS

The record IDs start by a letter indicating the location (M or V for Montreal and Vancouver) followed by the site class (C or E). The tests were performed in the order given in Table 2. For Montreal, tests were performed with simulated ground motion time histories generated for M6.0 earthquakes at short distances (< 20 km) and M7.0 earthquakes at larger distances (> 20 km) (Atkinson 2009). For Vancouver, ground motions representative of the three earthquake sources contributing to the seismic hazard in southwest British Columbia were used: shallow crustal, subduction deep in slab earthquakes expected at depths of 80-100 km, and large interface subduction earthquakes that are anticipated west of the Vancouver Island. The ground motions had been previously scaled in accordance with the provisions of the NBCC 2015 (NRCC 2015) as described in the Structural Commentaries (NRCC 2017), using the properties of the prototype buildings studied in Mottier et al. (2017). Because of the capacity of the shake table, the amplitude of the selected ground motions signals had to be reduced compared to the signals scaled to match the code spectrum. In Table 2, the penultimate column gives the ratio of the amplitude used to the code amplitude of the record. The last column details the ED devices that were installed on the test specimen for each ground motion signal. To investigate the influence of the ED device on the specimen's seismic response, five ground motion signals were used for all three ED devices: two for the Montreal configuration and three for the Vancouver configuration.

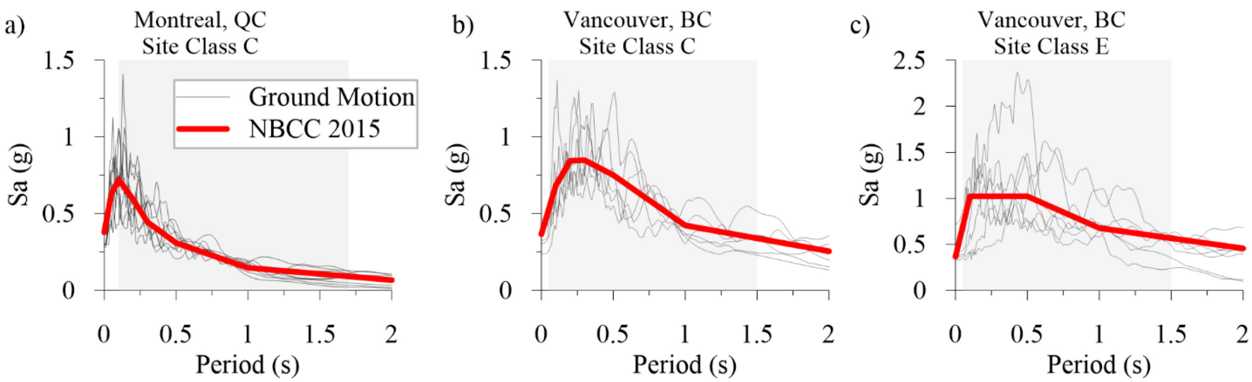

Figure 7 5 % damped acceleration spectra of the scaled ground motion records used in the shake-table tests.

PROPERTIES OF THE ROCKING FRAME

Once the rocking frame was mounted on the shake table and the instrumentation was installed, a series of preliminary tests were conducted to evaluate its dynamic properties: tests under 0-30 Hz white noise base excitation and pull-release tests. Both tests were conducted on the frame with fixed-base columns, for which column uplift was prevented by means of mechanical restraints to characterize the properties of the frame itself, and on the frame with uplifting column bases. The pull-release tests were performed by applying a small horizontal force at the roof level and suddenly releasing the frame using a trigger mechanism. In the tests with free column bases, the initial pull imposed an uplift of the column under tension. The test series with fixed base columns were first performed for the seismic weight configurations of both locations, starting with the configuration for Montreal.

A modal analysis was carried out with the Artemis Modal © software (SVS, 2014) to extract the structure's periods of vibration from the white noise test results, as well as damping values in the first lateral mode. Table 3 gives the measured periods of the specimen for the two configurations. The table also gives the periods predicted with the numerical model introduced in the last section of the article. The comparisons between measured and predicted values are discussed in that section.

Table 3 Measured and predicted natural periods of vibration (s) for the tested specimens

Mode	Montreal		Vancouver	
	Experimental value (Artemis)	Numerical Model	Experimental value (Artemis)	Numerical Model
Frame, 1st lateral mode	0.286	0.290	0.205	0.215
Frame, 2nd lateral mode	0.104	0.100	0.089	0.077
Floor Level, 1st vert. mode	0.190	0.196	0.200	0.196
Roof Level, 1st vert. mode	0.142	0.143	0.144	0.143

The frame for Vancouver has shorter lateral periods than for Montreal due to the lower seismic weight for that configuration. The periods of the vertical modes of vibration of the floor and roof structures are very close for both configurations, which was expected because the gravity framing and steel plates were the same. Because of the test sequence, slightly longer vertical periods were obtained at the floor and roof levels for the Vancouver-configuration, though. For instance, a 5.4% increase is noticeable at the floor level. This is attributed to the smoothing of the beam-to-column connections at both levels that occurred during the Montreal tests, prior to performing the preliminary tests for Vancouver. The periods measured in the tests were found to be longer than those predicted by numerical models when designing the test specimens with the similitude requirements. For instance, the anticipated first lateral mode periods were 0.197 s and 0.149 s for the Montreal and Vancouver configurations, respectively, and a first vertical mode period of 0.196 s was expected for both configurations. Visual inspection of the specimen revealed that the RBF column base plates were slightly bent, likely due to the welding process, which created a vertical gap between the foundation and base plates over the central part of the base plates. The base plates therefore acted as vertical springs between the column bases and the foundation plates. When these springs were included in the numerical model, it was found that a stiffness of 29 kN/mm was required to obtain numerically predicted periods that matched the measured values, as shown in Table 3. Damping values obtained from the white-noise tests varied between 5% and 7 % of critical damping in the first lateral mode; these higher than expected values being attributed to the low displacement amplitudes of such tests.

Figure 8 shows the results of one typical pull-release test for the frame with fixed base columns in Figure 8a and in the uplifting base condition in Figure 8b. As expected, the frame with rocking columns has a longer first-mode period of vibration compared to the specimen with fixed base columns: 0.62 s vs 0.26 s in the first cycle. However, the period for the rocking frame gradually shortens throughout the test as column uplift amplitude reduces. The tests with fixed base columns revealed higher than expected damping values, which were attributed to the friction between the RBF specimen and the lateral out-of-plane bracing system. That friction was then reduced by correcting the alignment of the RBF columns and the clearance between the test setup components. After these corrections, damping values in the first lateral mode extracted from the measured displacement time history responses to the pull-release tests using the log-decrement technique varied between 5% and 7 % of critical damping in the first lateral mode, still higher than the values generally assumed for bare-steel frame structures (2-3%).

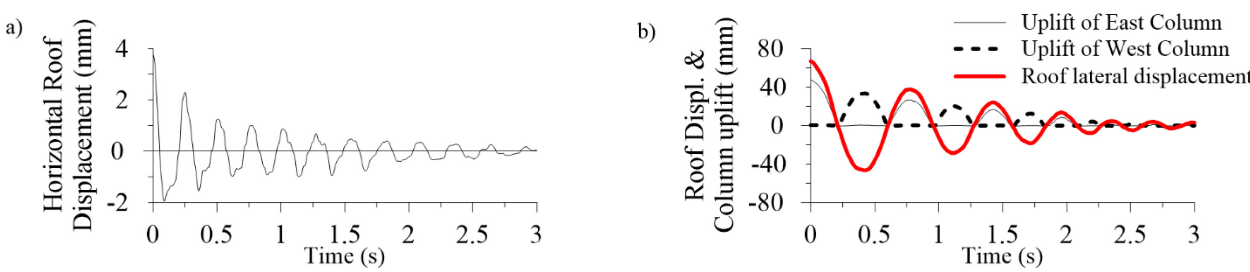

Figure 8 Time history responses from pull-release tests on the test frame for the Montreal configuration with: a) Fixed-base columns; b) Rocking-base columns (uplift = 47mm).

In the tests on the rocking frame, higher than expected friction was also observed. This time, its origin was attributed to friction between the column base plates and the blockers, as well as friction in the bolted beam-to-column connections. Friction at the column base was then reduced by greasing the rocking interface. This was done to isolate the rocking behaviour of the column itself and to ease the reproduction of the tests in the numerical models. However, no attempt was made to reduce the friction in the beam-to-column connections as it represents an inherent feature of steel structures likely to be present in actual buildings. This friction is beneficial as it dissipates energy during a seismic event.

Quasi-static cyclic tests were finally performed on the braced frame specimen by imposing with the shake table a cyclic displacement protocol at the frame base while restraining the lateral displacement at the frame roof level. These tests were performed with and without the ED elements installed at the column bases to verify the system cyclic response for all conditions before performing the seismic tests. The cyclic displacement had stepwise increasing amplitudes and was applied in one direction only. The measured force-displacement hysteretic responses for each ED system are shown in Figure 6. The frame exhibited a stable flag shaped force-displacement hysteretic response without the ED elements, and with all three ED systems. In each graph, the response of the specimen without the ED devices is also plotted for comparison. The results without ED elements show that the frame could exhibit stable self-centering response and possessed inherent energy dissipation capacity due to the friction in the beam-to-column connections. As foreseen, the force-displacement hysteretic behaviour of the devices significantly varies from one to another. The F device exhibited the highest energy dissipation capacity as slip occurred at a constant load in each cycle. The frame with the FS device showed the highest stiffness upon rocking. The FS device was also activated in each cycle but dissipated a smaller amount of energy compared to the friction device due to the friction spring force-deformation hysteretic response. Tests repeated at increasing displacement rates on the FS assembly showed no sensitivity to loading rate for this device. As expected, the YB developed nearly no compressive strength and accumulated permanent plastic deformations in tension in each cycle. As shown in Figure 6, the frame with the YB device exhibited lower resistance when the bars were reloaded in tension after yielding had occurred in a previous excursion. Due to this behaviour, it dissipated, overall, less energy than the two other devices.

OBSERVED SEISMIC RESPONSE

The response of the rocking frame under ground motion VE43 is presented in this section to examine the frame response and the influence of the three ED devices on that response. The response under that ground motion is representative of the results from the other tests performed for the Vancouver-configuration. Time history responses measured in the tests with the friction ED devices are shown in Figure 9. Similar behaviour was observed in the tests performed for the Montreal-configuration. The figure must be read from bottom to top. The figure presents the uplift at the base of the two RBF columns, the roof lateral displacement, the vertical acceleration measured at mid span of the roof level beam, the axial force in the West columns and West brace, the base shear and finally the shear and moment demands on the beams framing into the rocking columns at the floor level. Note that all results are presented as measured, in the model scale. Hence, time is reduced by the 0.3-time scale factor and the ground motion acceleration signal is amplified by S_{HA} = 5.56. The values under static loading before the start of the ground motion are included in all plots. In the figure, the vertical grey lines indicate the times of initiation and completion of the west column uplift excursions to see more easily the effects of column uplift and impact on the frame response.

Response of the Structure

As shown in Figure 9 a to c, the ground motion triggered alternately uplift response of both frame columns. The roof lateral displacement response is in phase with the column uplift and their amplitudes correspond, indicating that first mode (rocking) response governed roof displacements. For instance, the peak uplift of the west column reached 21.9 mm at t = 44.5 s, which resulted in a peak horizontal roof displacement of -32.6 mm. Assuming a rigid-body rocking response, the displacement from the measured column uplift would be 28.6 mm, the difference being due to elastic deformations of the frame members. In Figure 9d, the vertical acceleration at mid-span of the roof beam shows significant peaks that were triggered by impact of the RBF columns against the foundation plates after large uplift excursions. Such peaks reached as high as 4.2g at t = 45.9 s. Column impacts also caused the significant peaks of axial compression forces in the columns in Figure 9e, all peaks occurring at times when the columns returned into contact with the foundation. The highest axial force in the column reached 60 kN at t = 45.9 s, which corresponds to 2.12 times the column force under gravity loads alone. After each impact, the column forces reduced until the next impact occurred. In Figure 9e, it is observed that the force in the uplifted column, such as between t = 49.5 s and 49.75 s, oscillates at a period of 0.09 s, which corresponds to the vertical mode of vibration of the frame upon rocking. This mode was obtained from a modal analysis assuming a flexible support under one of the RBF columns (Mottier et al. 2020).

Figure 9f displays the axial force in the West brace at the first storey. The evolution of the brace axial force matches well the column uplift response, suggesting that brace forces are mainly governed by the frame first (rocking) mode response. Higher modes of vibration have less influence on the brace axial force than column axial force. However, it can be observed that each time the West column is in the uplifted position, higher mode effects are noticeable on the brace forces. Figure 9g displays the base shear measured during the tests. As shown, the base shear corresponds well to the brace axial force. In this figure, the horizontal dashed lines represent the positive and negative 51 kN base shears initiating column uplift (V_R) assuming static lateral seismic loads distributed as per the NBCC equivalent static force procedure. As can be noted, higher than expected base shears were recorded upon frame rocking. An additional study performed by the authors subsequent to this test program revealed that the high peak base shear values are due to the sudden change in boundary conditions at the column bases (Mottier et al. 2020). This study has confirmed that the frame first vertical vibration mode upon rocking governed the brace forces and base shears during uplift excursions.

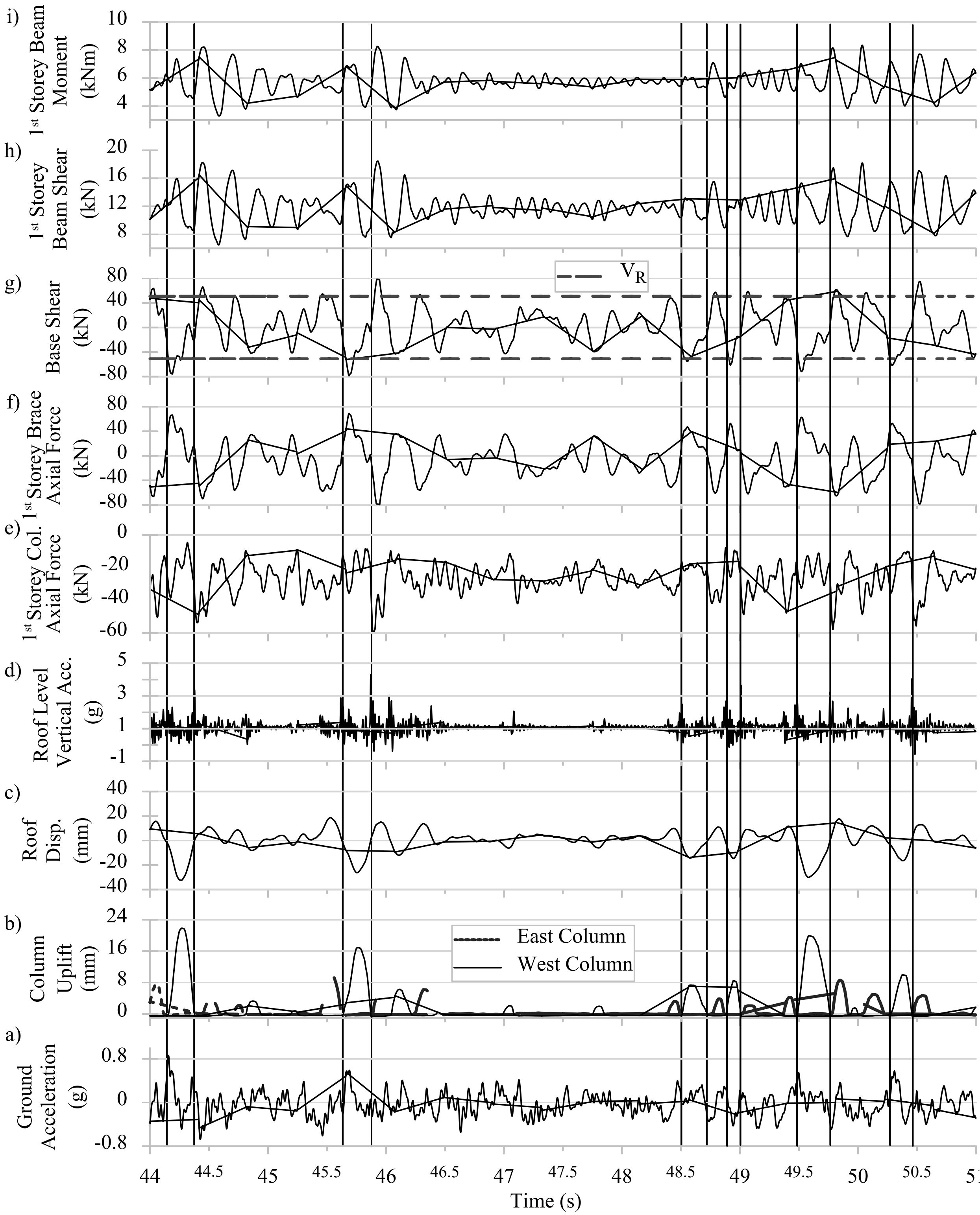

Figure 9 Response of the specimen to VE43 ground motion (Vancouver-configuration).

In Figure 9 h and i, excellent correlation can be obtained between the evolution of the shears and bending moments in the floor beam framing into the rocking column. From a modal analysis, it is found that shear and moment responses are governed by the first vertical mode of the plate-beam assemblies after rocking (T = 0.194 s). At t = 44.4, 45.9, 49.75, and 50.5 s, column impacts against the foundation caused a drastic increase in the beam shears and moments. This is due to the vertical inertia forces developing in the floor and roof assemblies when the downward course of the column is suddenly stopped by the foundation. After the impacts, both the shear and moment reduce as the vibrational energy is dissipated through friction. On all graphs showing the history of member forces it is noticed that all member force signals oscillate about the static value, without any offset that would suggest inelastic response and residual or permanent deformations.

Figure 10 displays the base shear and vertical base reaction *vs.* roof displacement responses under ground motion VE43 for the three ED devices. In all three cases, the curves are flag-shaped, typical of rocking frame structures. In all graphs, the horizontal dotted lines represent the values of the base shear and vertical base reaction obtained from moment equilibrium under a code static lateral force distribution. As was the case for the specimen with the friction, the frames with the FS and YB mechanisms exhibited significantly higher than expected base shears and vertical base reactions. This is again attributed to the vertical vibration vibrational response of the frame during column uplift, for the base shear, and to the large column axial forces resulting from column impact, for the vertical base reaction.

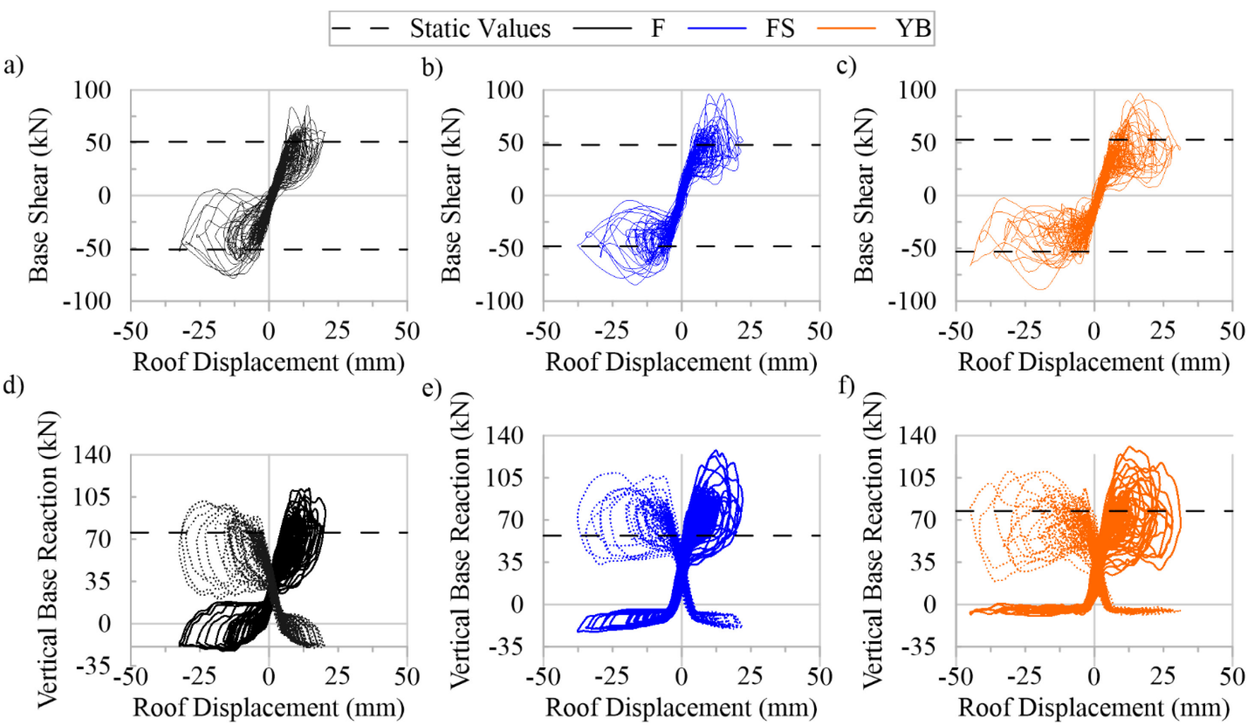

Figure 10 Responses of the rocking frame in the Vancouver configuration under the VE43 ground motion for the three ED systems: a-c) Base shear *vs* roof displacement responses; d-f) Columns vertical reaction *vs* roof displacement responses.

To study the influence of the ED devices on the frame response, a comparison of energy dissipated by each device as a function of time is presented in Figure 11 for eight different ground motions. Though the three devices had similar activation forces, they did not dissipate the same amount of energy during the earthquakes. The friction and friction spring devices were active in both compression and tension; conversely, the steel YB system dissipated energy only when the bars were incrementally stretched during larger uplift excursions. As shown, the friction device dissipated more energy than the other two EDs for five of the eight signals. The YB system dissipated the least energy in all cases but one. These differences are consistent with the different energy dissipation capacities anticipated from the cyclic force-displacement hysteric responses of Figure 6.

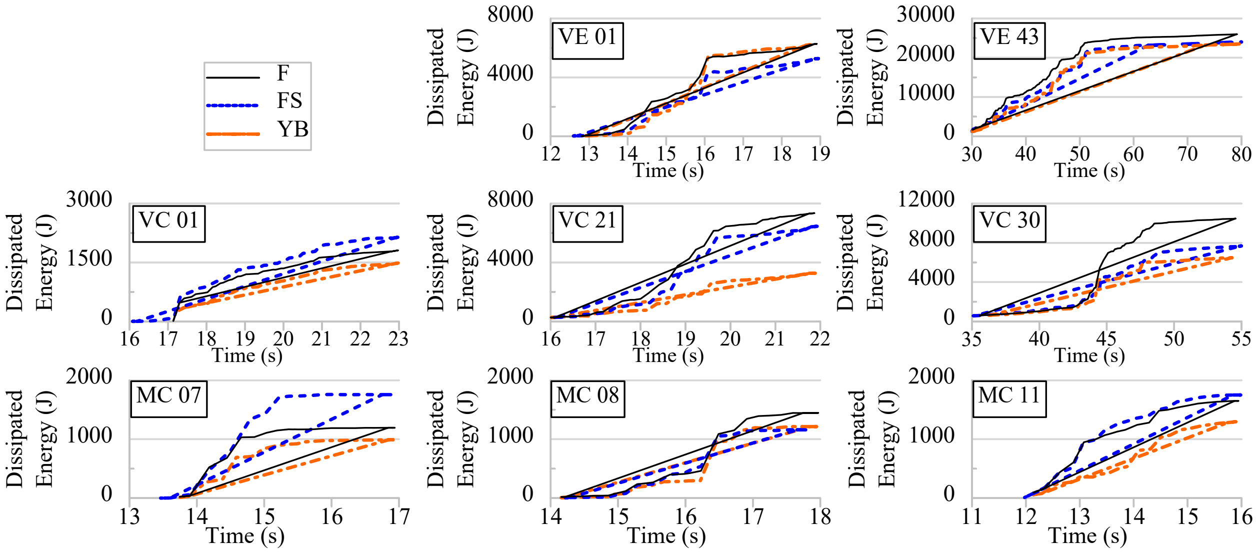

Figure 11 Effects of the ED devices; Energy Dissipation for 8 ground motions.

In Figure 12, partial time histories of the roof lateral displacements and beam shears are presented for four ground motions and all three ED devices. The results show that the friction device best controlled the horizontal and vertical displacements of the rocking frame. Under all ground motions but VC30, it resulted in the smallest peak lateral displacements. The YB mechanism was the least effective in controlling lateral displacements, likely because of its reduced energy dissipation capacity. Under all ground motions, the largest beam shears were observed with the ED mechanism producing the largest frame lateral displacements. This correlation could be expected as larger frame displacements induce higher column uplifts and, thereby, stronger column impacts. This correlation is examined further in the next section.

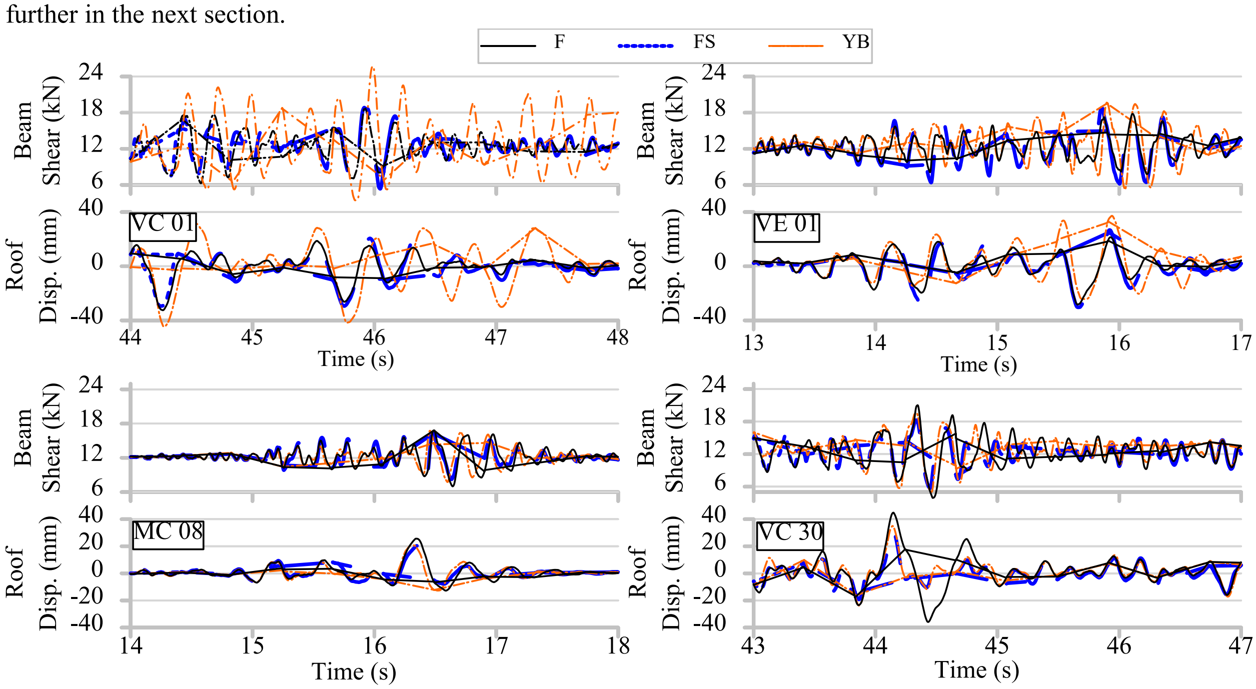

Figure 12 Roof lateral displacement and floor beam shear time histories for 4 representative ground motions and the three ED mechanisms.

TRENDS OBSERVED IN THE ROCKING FRAME RESPONSE

Peak values of key response parameters were determined for each of the tests performed under all ground motions listed in Table 2. Each peak value was then plotted as a function of the amplitude of the column uplift measured in the same test to examine the possible correlation between the two parameters. That correlation was studied only for the tests on the frame equipped with the friction ED device, as this mechanism is likely to be the preferred one in future applications in view of its higher efficiency. The parameters studied are the roof lateral displacement, the horizontal and vertical accelerations measured at the roof level at mid span of the frame beam, the axial compression force in the braces and the columns at the first storey, and the shears and bending moments in the floor beams framing into the rocking frame. The results presented in Figure 13 and Figure 14 are for the tests performed for the Montreal and Vancouver locations, respectively. In all graphs, a different colour is used for each ground motion. For each ground motion, results are presented for several uplift excursions covering the observed uplift range. For the roof displacements, the peak value measured during the earthquake is plotted against the concomitant column uplift. For all other parameters, the peak value is plotted against the column uplift reached in the uplift excursion that occurred just before the peak value was measured, i.e. the column uplift preceding the column impact causing the observed subsequent peak response value. For each response parameter, the linear regression parameters are given in the graphs.

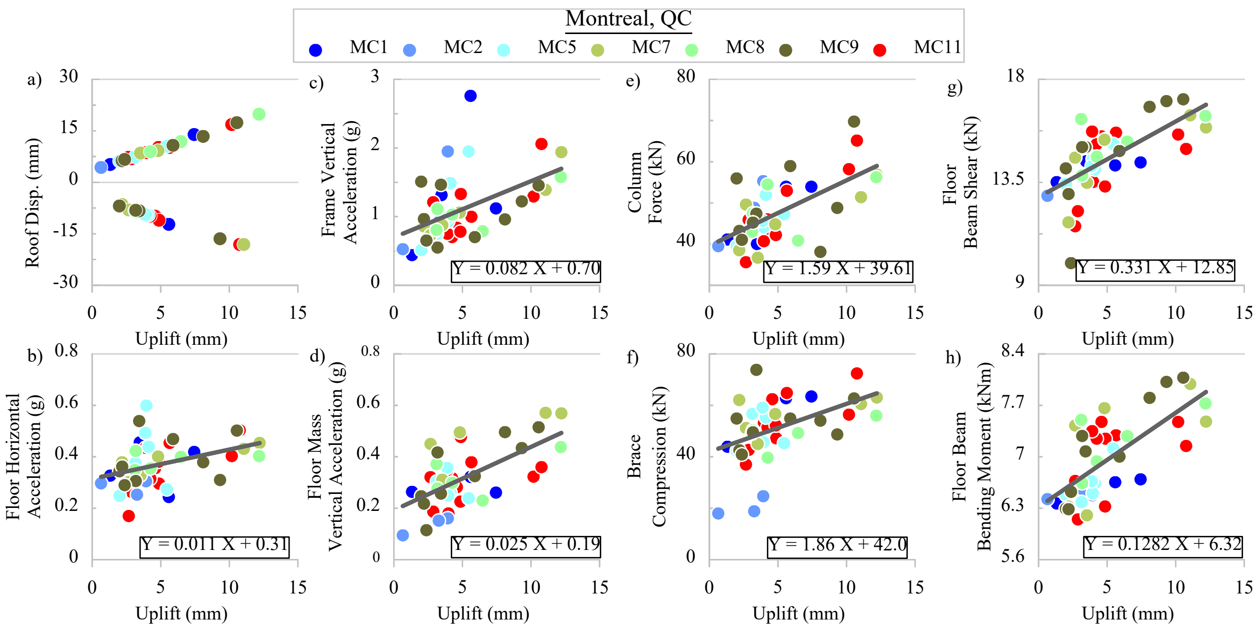

Figure 13 Variation of key response parameters with column uplift amplitude for the frame with friction ED devices in Montreal.

In Figure 13, peak column uplifts in the tests for the Montreal location ground motions are within the 0-15 mm range, whereas the frame for the Vancouver condition in Figure 14 experienced twice these values. Both figures confirm the strong and linear correlation between column uplift amplitudes and roof lateral displacements. If the rocking frame was infinitely stiff, the geometric ratio between the lateral displacement and column uplift would be equal to 1.30. The measurements give average ratios of 1.34 and 1.29 for Montreal and Vancouver, respectively, which corresponds very well to the theoretical values.

Although the data shows a large scatter, both horizontal and vertical accelerations after column impact generally increase with column uplift amplitude. As expected, brace and column axial loads, as well as shears and bending moments in beams, also steadily increase with the amplitude of column uplifts for both locations. For the force demands in beams, the slopes of the linear regressions for the Montreal and Vancouver locations are the same, suggesting that the amplitude of column uplift is the main factor governing peak vertical accelerations and force demands in gravity rocking frames. As for the forces in the frame members, the same trends are observed in Montreal and Vancouver. However, the slopes are more pronounced for the Montreal configuration, indicating that the effects of column impacts on the beam dynamic response is relatively more important for this configuration.

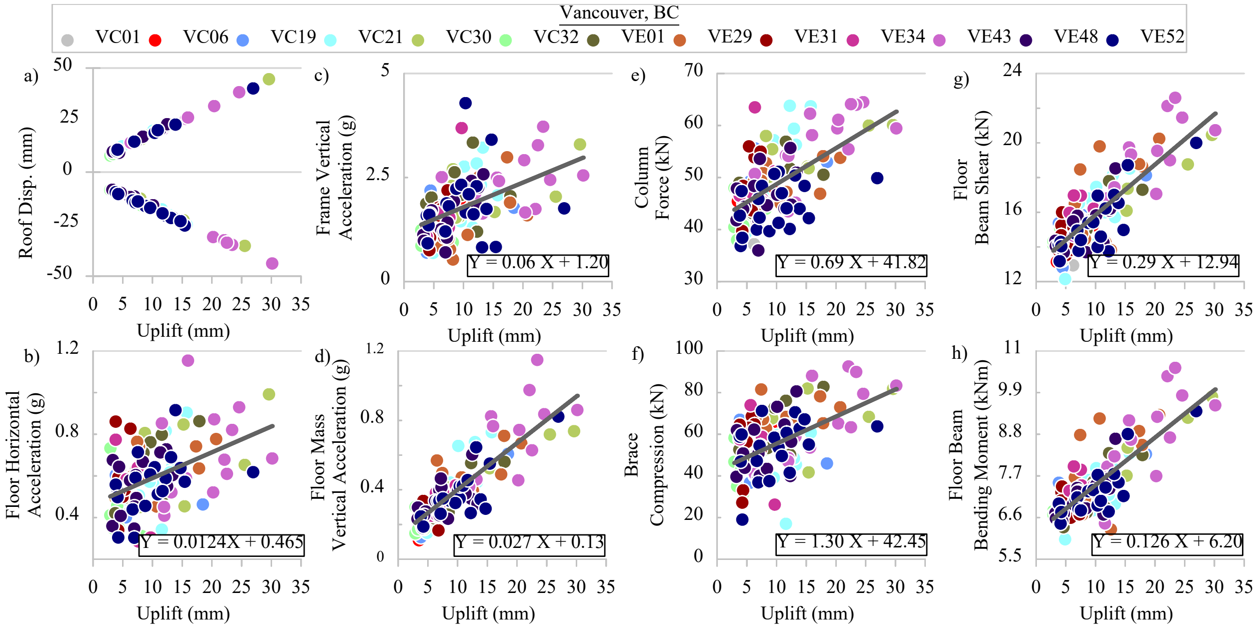

Figure 14 Variation of key response parameters with column uplift amplitude for the frame with friction ED devices in Vancouver.

NUMERICAL SIMULATIONS OF THE EXPERIMENTS

The numerical 3D-model shown in Figure 15 was built to replicate the frame response measured during the experiments. The model was created with the commercially available structural analysis software SAP2000 (CSI, 2019), and adapted from the numerical model proposed in a previous study (Mottier et al., 2017). The tests showed that all frame members remained in the elastic range and could therefore be modelled using elastic frame elements. The steel plates located at the floor and roof levels were reproduced with shell elements having the total thickness of the stacks. All gravity loads were specified as vertical masses assigned to the joints and shell elements so that the vertical inertia forces developing during the rocking cycles could be properly reproduced in the analyses. Rocking interfaces at the column bases were modelled using nonlinear vertical compression-only (gap) links. A stiffness of 29 kN/mm was assigned to these links to reproduce the flexibility induced by the flexural response of the initially bent base plates, as was discussed earlier. Partial rotational fixity was assigned at the ends of the transverse beam elements supporting the floor and roof masses to reproduce the observed rotational restraint of the beam-to-column connections. A rotational stiffness of 140 kN-m/rad was specified at both levels to obtain a good match between the measured and predicted first vertical vibration mode periods of the floor and the roof framing systems. For the Montreal configuration tests, the external seismic weight system was included in the model using a leaning column modelled with vertical truss elements. Gravity loads and horizontal masses corresponding to the weight of the steel plates of the system were assigned to the leaning column nodes at the floor and the roof levels. The horizontal struts linking the frame specimen and the seismic weight system were reproduced using truss elements with an axial stiffness corresponding to that of the struts. The horizontal displacement of the node at the base of the column reproducing the seismic weight system was constrained to be equal to that of the shake table, as was enforced in the laboratory by means of the horizontal frame on rollers supporting the seismic weight system that was horizontally connected to the shake table (Figure 4).

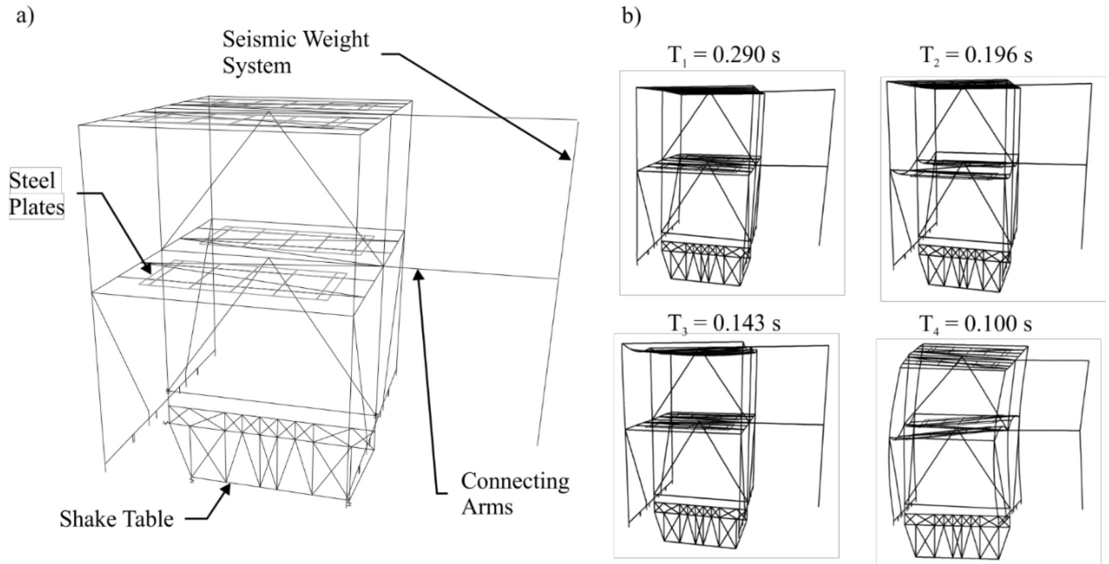

Figure 15 Numerical model built to replicate the experimental results; a) Montreal-configuration; b) Fundamental vibration modes.

The shake table used in the tests is mounted on frictionless horizontal linear hydrostatic bearings and has a total mass of 6.87 tons. The table was therefore included in the model to capture the behaviour of the entire specimen-earthquake simulator assembly, as shown in Figure 15. The table was modelled using elastic frame elements with high axial stiffness, while the table's hydrostatic bearings were modelled using vertical linear spring elements. The stiffness properties of these springs were adjusted to match the dynamic properties and the seismic behaviour of the bare table. The 5 m long HSS beams mounted transversely on the shake table to support the rocking and gravity frames were also included in the numerical model. As these beams were securely attached to the shake table, the displacements of their nodes located over the shake-table width were constrained to be same as those of the corresponding nodes of the shake table.

Modal analysis was first performed to obtain and compare the periods obtained from the model to those measured during the white noise tests. The model predictions are given in Table 3. As shown, excellent agreement could be achieved, with most differences being equal to or less than 5% of the experimental values.

Care was given to properly model the damping in the model for time-history analysis. Damping was specified as Rayleigh mass- and stiffness-proportional damping. Stiffness associated damping was implemented on the form of material damping properties for the frame and shell elements to avoid spurious damping developing in non-linear elements used at the rocking interface and for modelling the ED systems. After a few iterations, damping equal to, respectively, 4% and 7% of critical damping in the first and second lateral modes of the specimen in the fixed base condition, was selected to adequately predict lateral displacement and brace axial forces. These values were close to that obtained from the pull-release tests presented earlier. The seismic analyses were run as nonlinear time history analyses using the Newmark-beta integration scheme. Based on a previous study (Mottier et al., 2017), the time step in each analysis was set equal to half the time step of the ground motion file. No convergence issue was encountered. Prior to applying the ground motions, 1 g vertical acceleration was gradually applied using a linear ramp function to create the gravity loads from the vertical masses included in the model. The 1-g ramp had a duration of 1.5 s and a 2.0 s delay was left between the end of the ramp and the start of the ground motions to allow damping of the small vertical response induced by the application of the gravity acceleration.

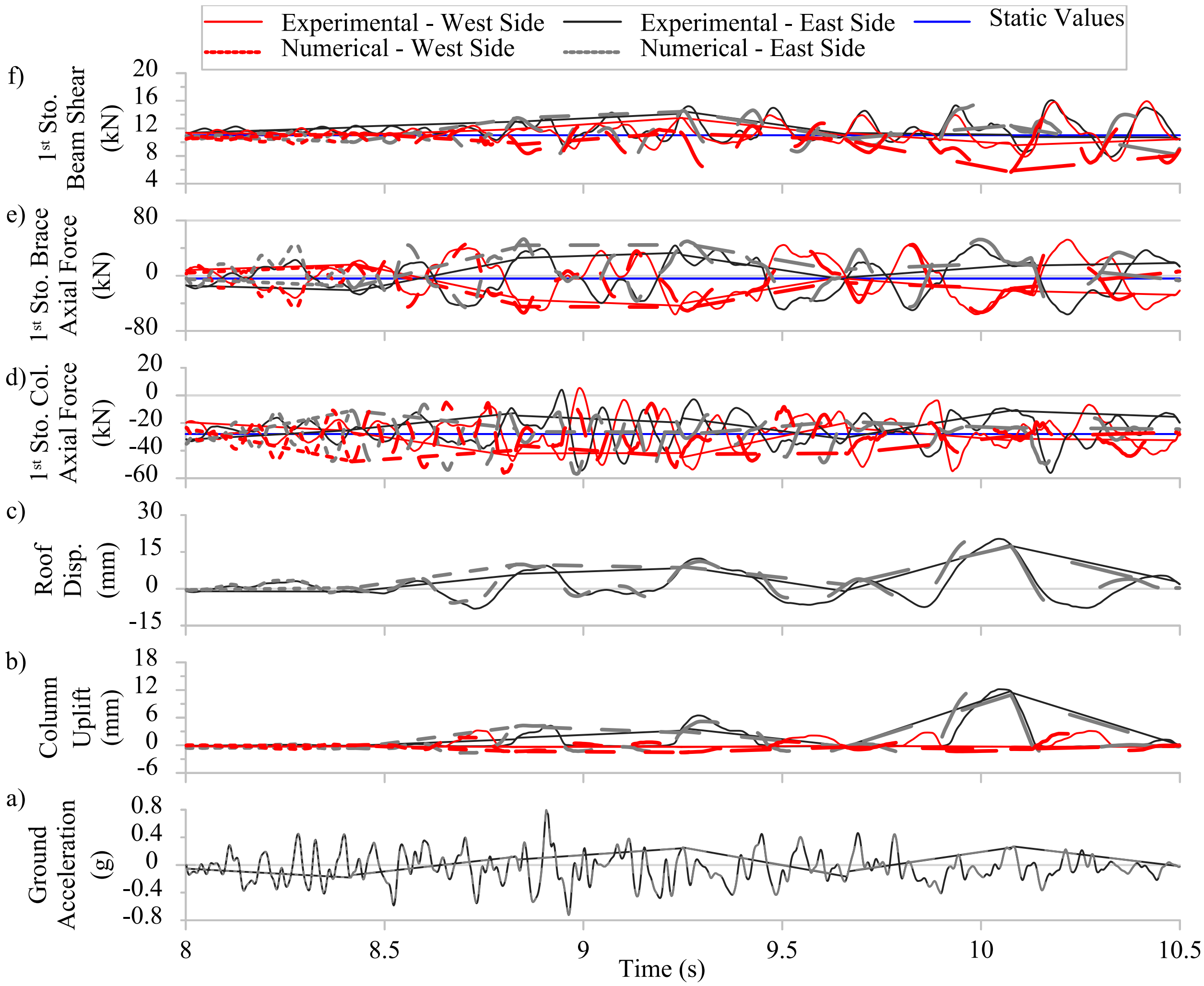

Figure 16 Comparisons between predicted and measured responses of the frame with friction EDs in the Montreal-configuration under MC8 ground motion.

Figure 16 shows the comparison between the numerical and experimental results for the frame with friction ED in the Montreal-configuration subjected to the MC8 ground motion. The figure presents the horizontal acceleration signal that was measured on the shake table and used as input in the analysis. The figure also shows the measured and computed histories of column uplifts, roof lateral displacement, and member forces. The values from static loading are included in the graphs showing the member forces. Excellent correlation was obtained between the experimental and numerical results for the column uplifts and the roof displacement. In Figure 16d, peak column axial load values are generally well predicted by the model, including the sudden changes at initiations of column uplift and after column impacts. Column forces from second mode response between rocking excursions were less pronounced in the tests. Excellent match can be observed between measured and computed brace forces in Figure 16e, both during and between column uplift excursions. For this parameter, second mode effects are also slightly overpredicted by the numerical model. In Figure 16 f, good correlation is obtained between the numerical and experimental shear forces in the out-of-plane beams at the storey level. Peak shear forces recorded following column impacts (e.g., at t = 9.25 s) or during column uplift (e.g., at t = 10.25 s) are predicted with good accuracy by the numerical model.

CONCLUSIONS

A shake-table experimental program was performed to examine the behaviour of a scaled two-storey gravity-controlled rocking steel braced frame and to confirm experimentally the results obtained from previous numerical simulations conducted by the authors. The self-centering capacity of the studied specimen was only conferred by the gravity loads carried by the frame. The focus of the test program was on the assessment of the effects of the impacts between the rocking columns and the foundation on member forces. The tests were performed on a half-scale model of the prototype structure. The effectiveness for drift control of three different energy dissipative devices was also evaluated and compared in the test program. Ground motions representative of the eastern and western seismic regions of Canada were applied in the tests.

Preliminary tests were performed to assess the dynamic properties of the frame and verify that the specimen behaved as intended. Some adjustments had to be made to correct higher than expected friction in the beam-to-column connections and at the rocking interfaces.

The following conclusions can be drawn on the effects of column impacts:

- Significant peaks of vertical accelerations are triggered each time the columns returned into contact with the foundation after a large uplift excursion. These accelerations reached values as high as 4.5 times the acceleration of gravity.
- The test results clearly showed that peak member forces in the frame increase linearly with the amplitude of the preceding column uplift, suggesting that additional member forces are caused by column impacts upon rocking. These amplified forces were observed in the rocking frame members as well as in the beams carrying gravity loads that frame into the rocking columns. This additional force demand must be properly assessed and incorporated in the design of GCRBFs to achieve safe seismic performance.
- The tests also revealed lateral and vertical reactions at the base of the rocking frame that exceeded the values predicted by static equilibrium. These higher forces are attributed to the vertical inertial loads that develop as the floor and roof masses are displaced vertically during rocking of the frame. These forces also need to be considered in the design of GCRBFs.

The comparison between the numerical and experimental results show excellent correlation between the numerical and the experimental results, proving that the proposed numerical model could predict the member force demands well in the rocking frame and, therefore, can be used in future research for the development of design procedures for GCRBFs.

The comparison of the responses obtained with the three different energy dissipative devices showed that member forces are not significantly influence by the type of ED system. However, the differences in the energy dissipation capacity of the ED devices, has a major impact on the amplitude of column uplift and lateral displacements. The results show that the friction type device, which had the greatest energy dissipation capacity, resulted in lower column uplifts and lateral displacements.

This study confirms the findings obtained from previous numerical simulations conducted by the authors. However, further research is needed to expand upon the results presented herein. In particular, the modelling of column impacts and their effects on the seismic response of gravity-controlled rocking braced frame should be performed to extend the findings of this study. Tests should be carried out on rocking frames supporting realistic floor slabs accounting for their continuity. The flexural stiffness and strength of the floor and roof framing systems should be considered to fully assess the overall seismic response of building structures with GRCBFs. Results from such additional experimental studies would help in the development of design guidelines to achieve effective gravity-controlled rocking braced frame buildings.

ACKNOWLEDGMENTS

Financial support for this research was provided by the Fonds de Recherche Nature et Technologies (FRQNT) of the Government of Quebec and the Natural Sciences and Engineering Research Council (NSERC) of Canada. The frame specimen was fabricated by Lainco Inc., Terrebonne, QC. The friction springs were donated by Ringfeder Power Transmission USA Corp., Westwood, NJ. The abrasive steel shim plates were donated by SSAB Swedish Steel Ltd., Delson, QC. The authors express their grateful appreciation to the technical staff of the Structural Engineering Laboratory at Polytechnique Montreal for their most valuable contribution.

REFERENCES

Atkinson, GM. Earthquake time histories compatible with the 2005 National building code of Canada uniform hazard spectrum. Canadian Journal of Civil Engineering, 2009, vol. 36, no 6, p. 991-1000.

ASCE. ASCE 41-13, Seismic Evaluation and Retrofit of Existing Buildings, American Society of Civil Engineers, Reston, VI, 2013.

Binder J, Christopoulos C. Seismic performance of hybrid ductile-rocking braced frame system. Earthquake Engineering and Structural Dynamics 2018; 47:1394–1415.

CSI. SAP 2000, Ver. 21, Integrated finite element analysis and design of structures basic analysis reference manual. Computers and Structures, Inc, Berkeley, CA, 2019.

Deierlein G, Ma X, Eatherton MR, Hajjar J, Krawinkler H, Takeuchi T, Kasai K, Midorikawa M. Earthquake resilient steel braced frames with controlled rocking and energy dissipating fuses. Steel Construction 2011; 4(3): 171-175.

Deierlein G, Ma X, Eatherton M, Krawinkler H, Hajjar J, Takeuchi T, Kasai K, Midorikawa M, Hikino T. Large-scale shaking table test of steel braced frame with controlled rocking and energy dissipating fuses. Proceedings 9th US National and 10th Canadian Conference on Earthquake Engineering, Toronto, Canada, Paper Nº 1248, 2010.

Dowdell DJ, Hamersley BA. Lions' Gate Bridge North Approach: Seismic retrofit. Proceedings of Behaviour of Steel Structures in Seismic Areas (STESSA) 2000 Conference, Montreal, Balkema, 2000.

Dyanati M, Huang Q, Roke D. Seismic demand models and performance evaluation of self-centering and conventional concentrically braced frames. Engineering Structures 2015; 84 368–381.

Eatherton MR, Hajjar JF. Hybrid simulation testing of a self-centering rocking steel braced frame system. Earthquake Engineering and Structural Dynamics 2014; 43(11):1725-1742.

Eatherton MR, Ma X, Krawinkler H, Deierlein GG, Hajjar JF. Quasi-static cyclic behaviour of controlled rocking steel frames. Journal of Structural Engineering 2014; 140(11).

HBM. Catman Data Acquisition Software. Hottinger Baldwin Messtechnik, 2000.

Hogg S. Seismically resilient building technology: examples of resilient buildings constructed in New Zealand since 2013. Proceedings 10th Pacific Conference on Earthquake Engineering Building an Earthquake-Resilient Pacific, Sydney, Australia, 2015.

Housner GW. The Behaviour of Inverted Pendulum Structures During Earthquakes. Bulletin of the Seismological Society of America 1963; 53(2): 403-417.

Huckelbridge AA. Earthquake simulation tests of a nine-story steel frame columns allowed to uplift. Report no. UCB/EERC-77/23, Earthquake Engineering Research Center, College of Engineering, University of California, Berkeley, CA, USA, 1977.

Jahnel L, Cole E. Design approach for friction spring dampers in steel framed buildings. Experiences from Christchurch/NZ. Proceedings 16th World Conference on Earthquake Engineering, Santiago, Chile, Paper Nº 675, 2017.

Kelly J, Tsztoo D. Earthquake simulation testing of a stepping frame with energy-absorbing devices. Report No. UCB/EERC-77/17, Earthquake Engineering Research Center, College of Engineering, University of California, Berkeley, CA, USA 1977.

Latham DA, Reay AM, Pampanin S. Kilmore Street Medical Centre: application of a post-tensioned steel rocking system. Proceedings Steel Innovations Conference 2013, Christchurch, New Zealand.
Mar D. Design examples using mode shaping spines for frame and wall buildings. Proceedings of the 9th US National and 10th Canadian Conference on Earthquake Engineering, Toronto, Canada, Paper Nº 1400, 2010.

Midorikawa M, Azuhata T, Ishihara T, Wada A. Shaking table tests on seismic response of steel braced frames with column uplift. Earthquake Engineering and Structural Dynamics 2006; 35:1767-1785.

Mottier P, Tremblay R, Rogers C. Seismic retrofit of low-rise steel buildings in Canada using rocking steel braced frames. Earthquake Engineering and Structural Dynamics 2017; 47(2): 333-355.

Mottier P, Tremblay R, Rogers C. Full-scale impact tests of columns for rocking steel braced frames. Proceedings 12th Canadian Conference on Earthquake Engineering, Quebec, Canada, 2019.

Mottier P, Tremblay R, Rogers C, Wiebe L. Influence of vertical masses on the response of gravity-controlled rocking braced frames. Proceedings 17th World Conference on Earthquake Engineering, Sendaï, Japan, 2020 (Submitted).

NRCC. National Building Code of Canada 2015, 14th ed. National Research Council of Canada, Ottawa, ON, 2015.

NRCC. Structural Commentaries (User's Guide – NBC 2015: Part 4 of Division B), 4th ed. National Research Council of Canada, Ottawa, ON, 2017.

Pollino M, Bruneau M. Dynamic seismic response of controlled rocking bridge steel-truss piers. Engineering Structures 2008; 30:1667-1676.

Pollino M, Bruneau M. Seismic testing of a bridge steel truss pier designed for controlled rocking. Journal of Structural Engineering 2010; 136(12):1523-1532.

Priestley MJN, Evison RJ, Carr A. Seismic Response of Structures Free to Rock on their Foundations. Bulletin of the New Zealand National Society for Earthquake Engineering 1978; 11(3).

Sause R, Ricles JM, Roke DA, Chancellor NB, Gonner NP. Seismic performance of a self-centring rocking concentrically-braced frame. Proceedings 9th US National and 10th Canadian Conference on Earthquake Engineering, Toronto, Canada, Paper Nº 1330, 2010.

Steele TC, Wiebe LD. Collapse risk of controlled rocking steel braced frames with different post-tensioning and energy dissipation designs. Earthquake Engineering and Structural Dynamics 2017; 46:2063-2082.

SVS. *ARTeMIS Modal Pro 3.0*. Structural Vibration Solutions, Aalborg East, Denmark, 2014.

Tipping-Mar. Packard foundation headquarter building. Los Altos, CA, 2012. http://www.tippingmar.com/projects/project_details/43

Tran BT, Kasai K, Sato T, Oohara K, Shao L. JSSI Manual for building passive control technology; Part-7 Stepping Column System. Proceedings 13th World Conference on Earthquake Engineering, Vancouver, Canada, Paper Nº 5059, 2004.

Tremblay R, Poirier L-P, Bouaanani N. Innovative viscously damped rocking braced steel frames. Proceedings 14th World Conference on Earthquake Engineering, Beijing, China, Paper Nº 05-01-0527, 2008.

Wiebe L, Christopoulos C, Tremblay R, Leclerc M. Mechanisms to limit higher mode effects in a controlled rocking steel frame. 1: Concept, modelling, and low-amplitude shake table testing. Earthquake Engineering and Structural Dynamics 2013; 42(7): 1053-1068.